Pergamon

0956-7151(95)00247-2

Acta mater. Vol. 44, No. 3, pp. 1001–1010, 1996
Elsevier Science Ltd
Copyright © 1996 Acta Metallurgica Inc.
Printed in Great Britain. All rights reserved
1359-6454/96 $15.00 + 0.00

Si_3N_4–Al_2O_3/Si_3N_4–Y_2O_3 COUPLE DIFFUSION SYSTEM

S. MELLO CASTANHO[1,†], J. S. MOYA[1], G. S. BLUGAN[2] and M. J. REECE[2]

[1]Instituto de Ceramica y Vidrio—CSIC, 28500 Arganda del Rey, Madrid, Spain and
[2]Materials Department, QMW College, University of London Mile End Road, London E1 4NS, U.K.

(Received 19 April 1995; in revised form 18 May 1995)

Abstract—The behaviour of the additives Al_2O_3 and Y_2O_3 on the microstructure of Si_3N_4 and Si_3N_4–ZrO_2 doped materials was studied using couple diffusion systems (Si_3N_4–Al_2O_3/Si_3N_4–Y_2O_3). After heat treatments, the line profile for Al and Y was determined. The secondary intergranular phases were identified by XRD and TEM analysis. The influence of the chemical composition of the intergranular glassy phase in the final microstructure after sintering was observed. The drastic effect of the Y_2O_3 and ZrO_2 on the α-β Si_3N_4 transformation, β-Si_3N_4 average grain size, density and on the crystalline secondary grain boundary phases has been investigated. The main conclusions are that the presence of zirconia drastically decreases the viscosity of the glassy phase developed in the Si_3N_4–Al_2O_3 system; when both Y_2O_3 and ZrO_2 are present in this system devitrification of grain boundary amorphous phase takes place; when zirconia is present in the Si_3N_4–Y_2O_3 system no unwanted quaternary crystalline phases are formed.

1. INTRODUCTION

The production of silicon nitride based ceramics is of considerable interest because of their unique combination of chemical, physical and mechanical properties, which makes them an important class of materials for a wide range of applications at elevated temperatures [1]. However, as it is a covalently bonded solid, the self-diffusivity of pure silicon nitride is very low and consequently it is very difficult to sinter to maximum density [2, 3]. For this reason, sintering additives are required to form a liquid phase at the sintering temperature in order to achieve highly dense silicon nitride based materials [4–9]. Oxide additives or a combination of them, such as MgO [3]; Y_2O_3–Al_2O_3 [5, 10]; ZrO_2 [11, 12]; Y_2O_3–Nd_2O_3 [13] and other rare earth oxides [4, 14], are used to promote densification in the sintering process. After sintering, these additives generally remain as grain-boundary glassy phases. These phases deteriorate the high-temperature mechanical properties of sintered silicon nitride, such as their creep resistance and strength [14, 15] and also affect their oxidation behaviour. The high temperature performance depends primarily on the composition of the intergranular phases, and their distribution.

Although a large number of papers have been published on the effect of additives and dopants on microstructure, grain boundary glassy phase and hence on the high temperature mechanical performance of silicon nitride based materials, confusion and contradictory results about the role of impurities and additives in the microstructural feature and properties of silicon nitride compacts is still evident in the literature [4–9].

In the present work we studied this problem using a completely different experimental approach using a couple diffusion system. The main advantage of this experimental route is in the fact that in one single specimen we have a range of compositions.

Al_2O_3 and Y_2O_3 oxides have been found to enhance the densification and mechanical behaviour of the Si_3N_4. On the other hand, recent investigations [12] have pointed out that the presence of ZrO_2 as a dopant in Si_3N_4 containing yttria or alumina as sintering additive promotes the devitrification of the remaining glassy phase in the sintered compact.

The aim of the present investigation is to study the microstructure of ZrO_2 doped silicon nitride containing Y_2O_3 and Al_2O_3 additives using a couple diffusion system.

2. EXPERIMENTAL PROCEDURE

α-Si_3N_4 powder (LC-12SX, H. C. Starck, Germany), with C (1800 ppm), Fe (54 ppm) and Al (45 ppm) impurities; 0.46 μm average particle size; specific surface area of 18 m^2/g; and an oxygen content of 1.75 mass%, was used. Al_2O_3 (Condea, Germany), with 99.99 mass% purity; 0.4 μm average particle size; 9.5 m^2/g specific surface area and Y_2O_3 (Mandoval, U.K.), 99.99 mass% purity content; 3.5 μm average particle size and 6.85 m^2/g specific surface area, were used as sintering aids. Two compositions from which the experimental couples were prepared: Si_3N_4 + 5 mass% Y_2O_3 labelled SNY and Si_3N_4 + 5 mass% Al_2O_3 labelled SNA.

†On leave from: IPEN-CNEN/SP-CP11049, Cidade Universitária-USP, São Paulo-Brazil.

The mixing of the powders was performed in an attritor lined with Teflon to avoid contamination in isopropanol-2 using 1–2 mm sized, (Mg–PSZ) balls as milling media for 2 h. After drying (80°C/12 h) and sieving ($<60\ \mu m$), both powders were subsequently uniaxially pressed in a 20 mm diameter die in order to obtain a couple system formed by the two compositions spatially separated by a plane. This specimen is referred to as SNA/SNY–ZrO_2.

Subsequently this couple was submitted to isostatic pressing at 200 MPa. Then the pellets were sintered in a BN crucible with a Si_3N_4 powder protective bed at 1750°C for 2 h in N_2 gas. After sintering some samples were annealed at 1300°C for 48 h. The same procedure was performed using 2 mm sized silicon nitride balls as the milling media, for comparison purposes. This specimen is referred to as SNA/SNY–Si_3N_4.

The microstructure of the samples were studied by optical microscopy, scanning electron microscopy (SEM) and transmission electron microscopy (TEM).

The different phases in the couple specimens were detected by performing X-ray diffraction (XRD) studies at different depths parallel to the SNA–SNY interface.

To study the compositional change across the couple specimens, the cross-sections of the SNA/SNY couple were polished down to 1 μm. Their microstructures were then studied using a SEM with microprobe analysis wavelength dispersion spectrometry (WDS, JMS-6400) with two spectrometers—Crystal PET for Y ($\lambda = 6.4480$, $K\alpha_1$) and TAP for Al ($\lambda = 8.34013$, $K\alpha_{1+2}$).

The X-ray diffraction studies were performed using a Siemens D5000 diffractometer. Analyses were performed at different depths parallel to the interface plane. The samples were ground and polished sequentially from the SNA surface and XRD patterns recorded. The specimens used for optical microscopy and SEM analysis were prepared by diamond polishing a section perpendicular to the couple interface. This enabled the microstructure as a function of changing composition to be studied.

TEM specimens were prepared from sections cut perpendicular to the interface of the couples. These were then ground and polished on both sides to produce specimens approx. 50 μm thick. Copper hole grids were then glued over the area of interest. These specimens were then ion beam thinned to electron transparency at 5 kV using argon ions. The specimens were studied in a JEOL 2010 instrument (at 200 keV) equipped with an ultrathin window energy dispersive X-ray detector (EDS).

3. RESULTS

Wet chemical analysis of $Si_3N_4 + Y_2O_3$ (5 mass%) and $Si_3N_4 + Al_2O_3$ (5 mass%) homogeneous mixtures after attrition milling with Mg–PSZ balls gave a zirconia doping of 1.27 and 1.21 mass%, respectively. This zirconia is responsible for some of the secondary phases identified in the XRD and TEM studies.

Figure 1 shows an optical micrograph of the cross section of the sintered SNA/SNY–ZrO_2 couple and the corresponding composition line profiles for Y and Al. These results show that Y diffused into the SNA layer to a depth of approx. 800 μm from the SNA–SNY interface. The Al diffused approximately 400 μm into the SNY layer. Also included in Fig. 1 is a plot of the surface porosity of the couple as a function of position. The relatively low porosity of the SNA side compared to the SNY side of the couple

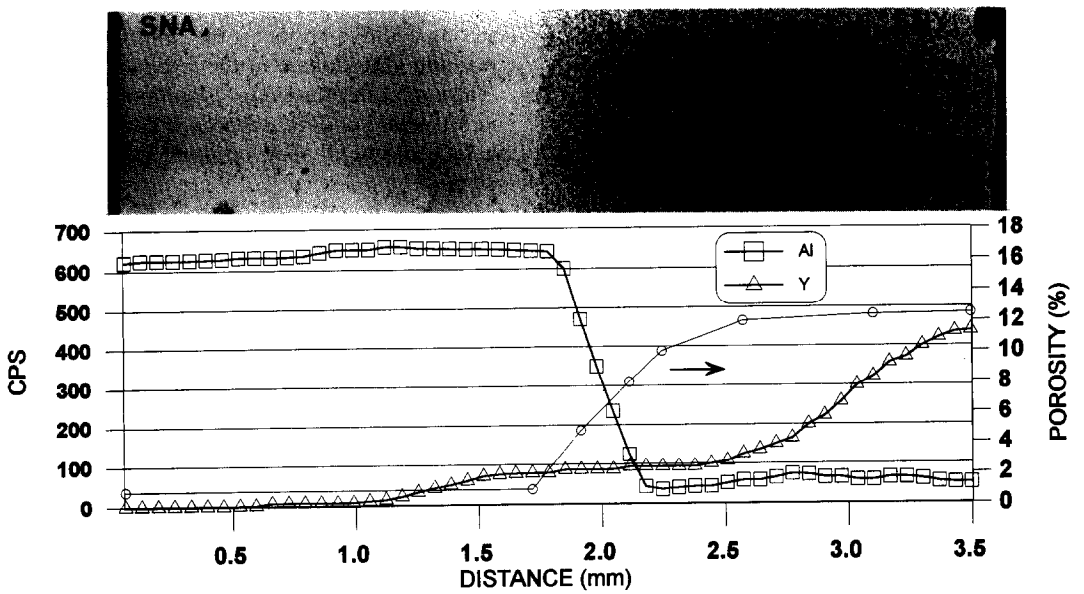

Fig. 1. Optical micrograph, Y and Al compositional line profile and porosity profile across the polished cross-section of the SNA/SNY–ZrO_2 couple.

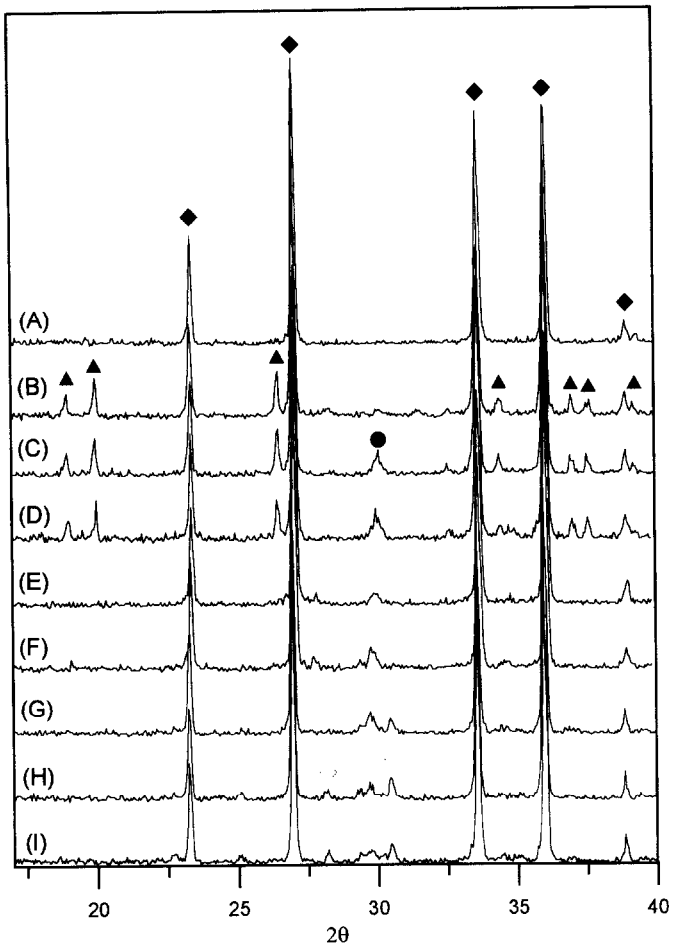

Fig. 2. XRD patterns at different depths through the SNA/SNY–ZrO_2 couple. From the SNA surface to the SNY surface: (A) on SNA surface; (B) 420 μm; (C) 800 μm; (D) 1000 μm; (E) 1380 μm; (F) 1610 μm; (G) 2030 μm; (H) 2250 μm; (I) 2510 μm. [Legend: (◆) β-Si_3N_4, (▲) Si_2N_2O, (●) $Zr_3Y_4O_{12}$, (◇) Y_2SiO_5].

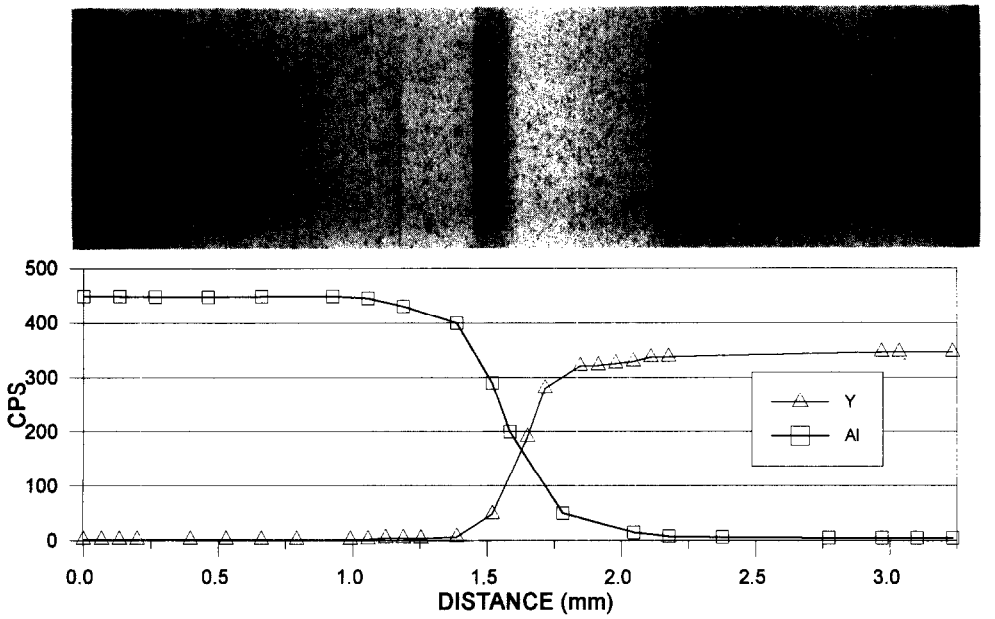

Fig. 3. (a) Optical micrograph, Y and Al compositional line profile across the polished cross-section of the SNA/SNY–Si_3N_4 couple distribution.

and the greater diffusion of Y compared to Al across the couple interface is indicative of a more effective liquid phase sintering on the SNA side of the couple. This is presumably a consequence of the Al_2O_3-rich intergranular phase in the SNA side having a lower viscosity compared to the intergranular phase in the SNY side during sintering.

Figure 2 shows the XRD depth profile patterns for the couple prepared using Mg–PSZ balls after annealing (SNA/SNY–ZrO_2). The interface for the couple corresponds to $\approx 1600\,\mu m$ from the reference SNA surface. The major phase throughout the couple is β-Si_3N_4, no α-Si_3N_4 was detected. In the SNA side of the couple silicon oxynitride (Si_2N_2O) is present in an appreciable amount as a second phase to a depth of approx. $1000\,\mu m$ from the SNA surface. At a depth of $800\,\mu m$ from the SNA surface and throughout the remainder of the couple the hexagonal structured $Zr_3Y_4O_{12}$ phase was detected as a second phase. This observation is consistent with the compositional line profile study (Fig. 1) which shows significant diffusion of Y to this depth into the SNA side of the couple. On the SNY side of the couple the monoclinic structured Y_2SiO_5 phase was also detected throughout. The annealing treatment did not have a significant effect on the relative proportion of phases present compared to the as sintered material.

Figure 3 shows the optical micrograph of the cross-section of the sintered SNA/SNY–Si_3N_4 couple and the corresponding composition profile for Y and Al. The Y diffused into the SNA layer to a depth of only $\approx 50\,\mu m$ from the interface. The Al diffusion shows a similar trend to that observed in the ZrO_2-doped sample (Fig. 1).

Figure 4 shows the XRD profile patterns for the couple prepared using the Si_3N_4 milling balls after annealing treatment (SNA/SNY–Si_3N_4). The interface for the couple corresponds to $\approx 1450\,\mu m$. In this particular case a significant fraction ($\approx 16\%$), of α-Si_3N_4 was detected on the SNA side of the couple, a similar result was observed by Goto and Thomas [16] in $Si_3N_4 + 10$ mass% Al_2O_3 composition. This phase was present at a relatively uniform content up to the interface of the couple. The XRD patterns for the SNY side of the couple show no peaks corresponding to the Y_2SiO_5 phase detected in the

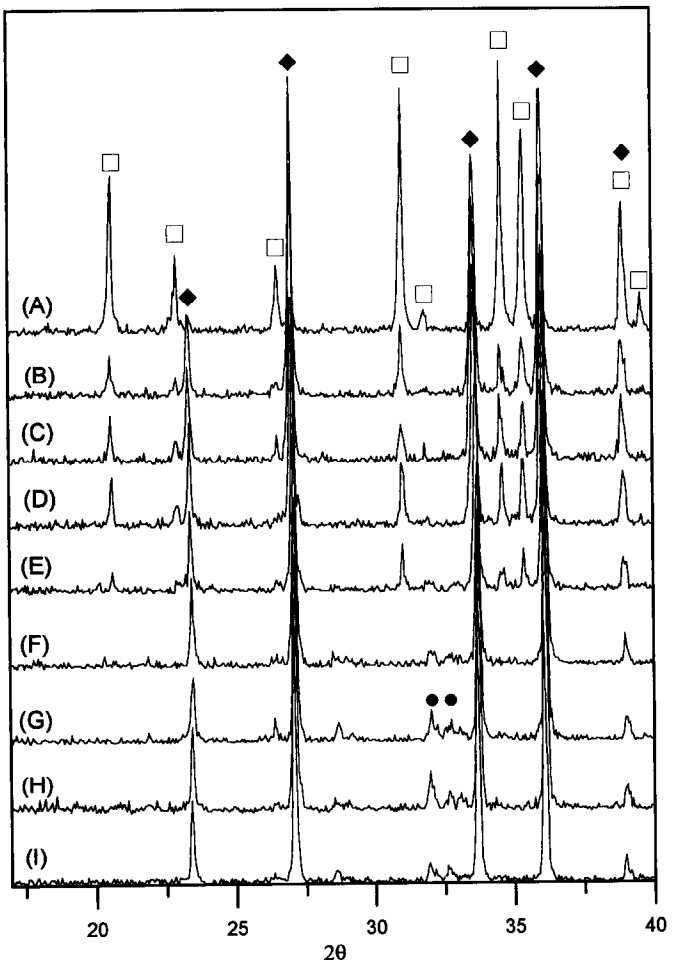

Fig. 4. XRD patterns at different depths through the SNA/SNY–Si_3N_4 couple. From SNA surface to the SNY surface: (A) on SNA surface; (B) $400\,\mu m$; (C) $650\,\mu m$; (D) $1180\,\mu m$; (E) $1430\,\mu m$; (F) $1600\,\mu m$; (G) $2180\,\mu m$; (H) $2630\,\mu m$; (I) SNY surface. [Legend: (□) α-Si_3N_4, (◆) β-Si_3N_4, (●) $Y_2Si_3N_4O_3$].

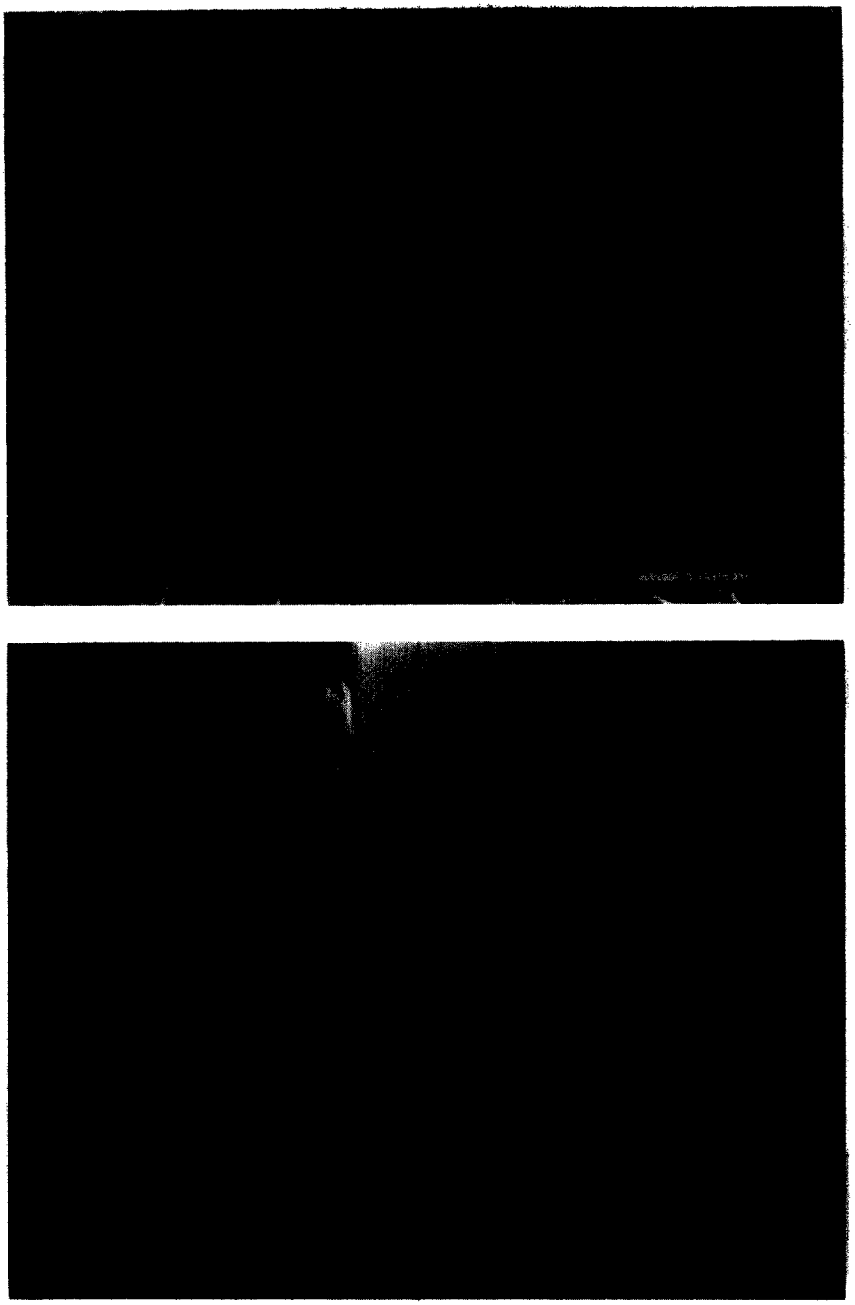

Fig. 5. (A) SEM micrograph showing the plasma etched microstructure of SNA side of the SNA/SNY–ZrO_2 couple at a depth of $\approx 600\,\mu m$ from the SNA surface. (B) TEM dark field micrograph showing the present of intergranular glassy phase.

SNA/SNY–ZrO_2 specimen. Conversely a quaternary compound ($Y_2Si_3N_4O_3$) is now present. Because ZrO_2 was not present to react with the Y_2O_3 to form $Zr_3Y_4O_{12}$, the Y_2O_3 content of the liquid phase was presumably higher than for the SNA/SNY–ZrO_2 couple and consequently phases with a higher Y_2O_3 content were formed.

SEM examination of the plasma etched SNA/SNY–ZrO_2 specimen corresponding to $\approx 600\,\mu m$ from the SNA surface showed that the β-Si_3N_4 grains were mostly small equiaxed ($\approx 0.5\,\mu m$ diameter) with only very few grains being elongated (Fig. 5). The Si_2N_2O phase had a similar grain size to the β-Si_3N_4 phase. It was possible to distinguish Si_2N_2O grains by the fact that they were faceted and often contained planar defects [17] (Fig. 6). X-Ray microanalysis of Si_2N_2O grains showed that they always contained a small proportion of Al as Al_2O_3 in solid solution. At $\approx 300\,\mu m$ from the SNA surface, the ZrO_2 present from the ball milling was apparent as dense particles which tended to be grouped into pockets (Fig. 7). Analysis of the Zr phase revealed that it was present

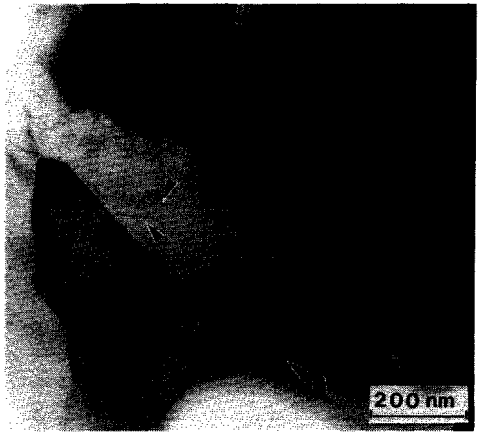

Fig. 6. TEM micrograph showing Si_2N_2O grains, planar defects have been highlighted in one of the grains. **G** = Pocket glassy.

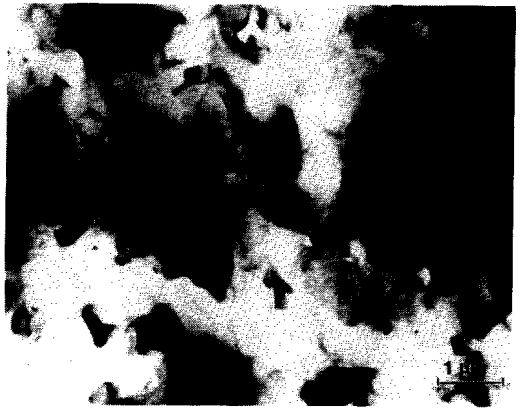

Fig. 7. TEM micrograph showing in the SNA side of the SNA/SNY + ZrO_2 couple. Pocket of ZrO_2 particles (dark) surrounded by β-Si_3N_4 and Si_2N_2O grains (BF image).

Fig. 8. TEM micrograph showing Y_2SiO_5 crystallized as intergranular phase near the SNA–SNY interface in the SNA/SNY + ZrO_2 specimen, BF image with corresponding SADP.

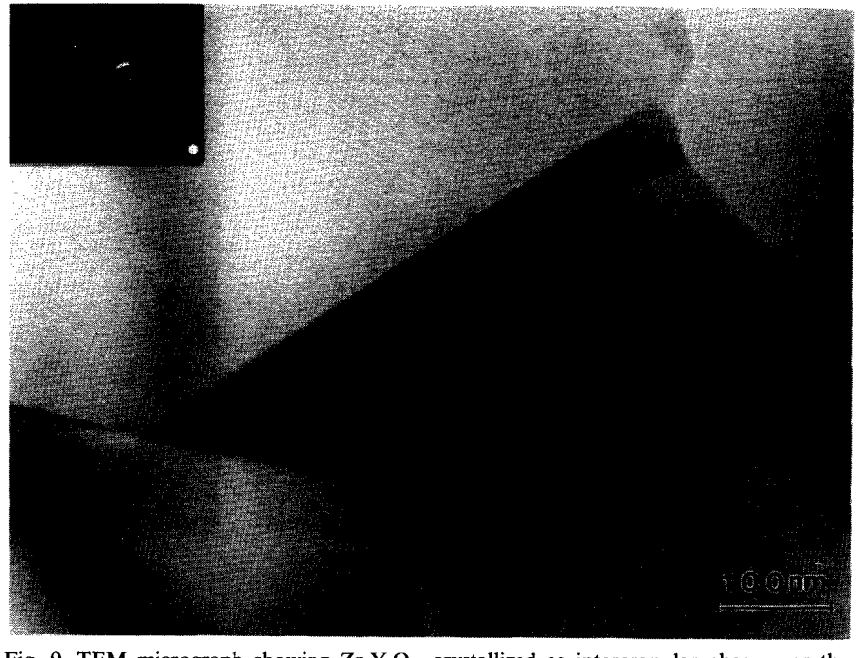

Fig. 9. TEM micrograph showing $Zr_3Y_4O_{12}$ crystallized as intergranular phase near the SNA/SNY interface in the SNA/SNY–ZrO_2 specimen, BF image with corresponding SADP.

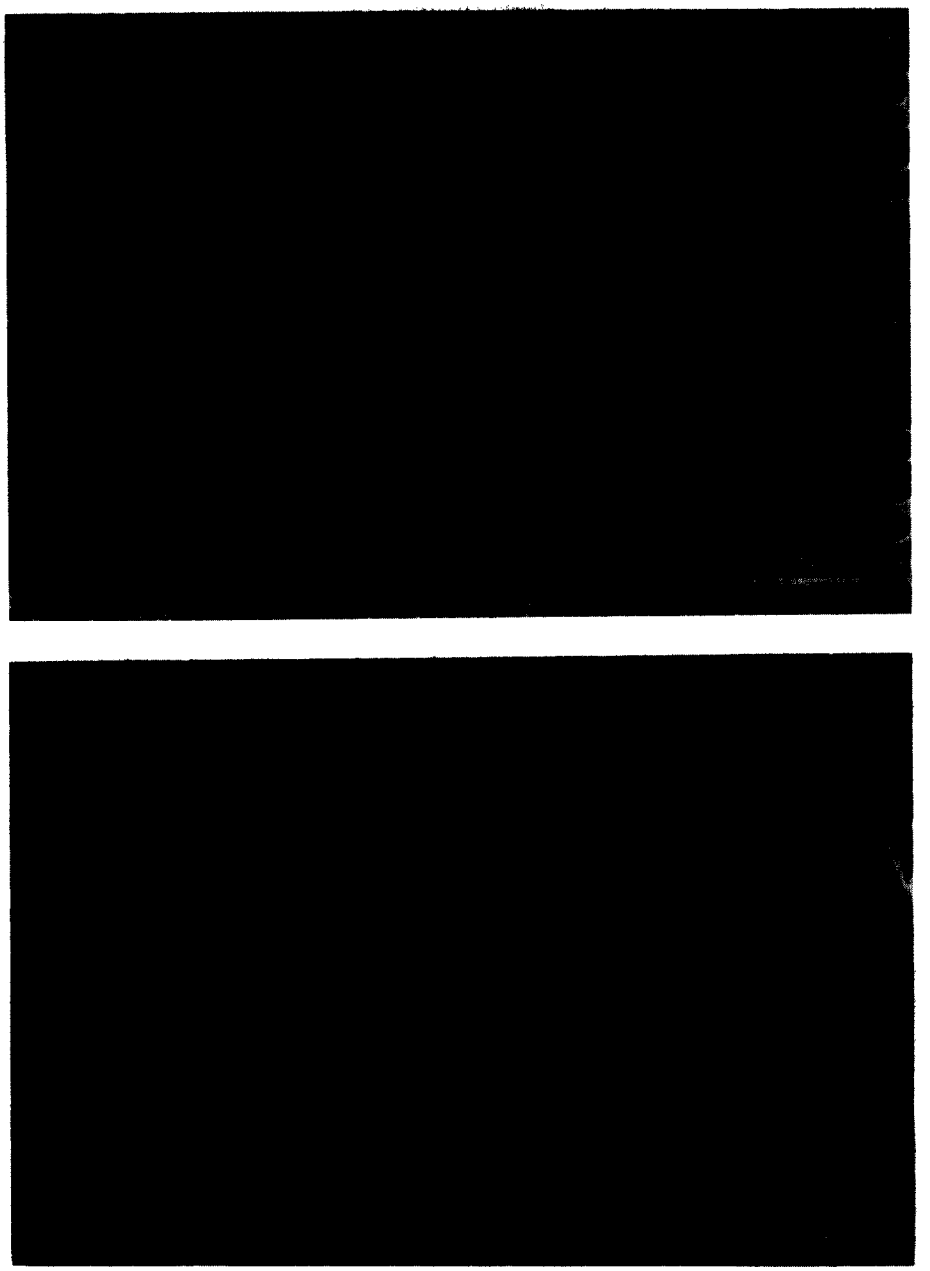

Fig. 10. SEM micrograph showing the plasma etched microstructure corresponding to (A) interface region and to (B) SNY side of SNA/SNY + ZrO_2 couple.

as ZrO_2. The ZrO_2 particles were irregularly shaped and fitted between surrounding Si_2N_2O and β-Si_3N_4 grains. The morphology of the particles suggests that they formed by precipitation from a transient ZrO_2 containing liquid phase. The ZrO_2 phase was presumably not detected in the XRD patterns (Fig. 2), because of its relatively low content, ≈ 1 mass%. The intergranular phase was amorphous and contained Si, Al and O. The amorphous intergranular phases showed good grain boundary wettability as evidenced on the small dihedral angles formed at triple points (Fig. 5). Other than close to the SNA surface ($\approx 300\,\mu$m) the ZrO_2 phase could no longer be detected.

In the regions closer to the SNA–SNY interface the intergranular material was predominantly crystalline and consisted of Y_2SiO_5 and $Zr_3Y_4O_{12}$ phases (Figs 8 and 9, respectively). The composition of the amorphous intergranular phase contained increasing amounts of Y and Zr in regions approaching the interface. No amorphous intergranular phase could be detected very closed to the interface. A general view of the microstructure is given in Fig. 10(A).

Fig. 11. BF image of a pocket of crystallized $Zr_3Y_4O_{12}$ phase surrounding small β-Si_3N_4 grains in the SNY side of the SNA/SNY–ZrO_2.

In the SNY side of the SNA/SNY–ZrO_2 couple a significant proportion of the β–Si_3N_4 grains were elongated with dimensions typically of $\approx 0.5 \times 3.0\ \mu m$ [Fig. 10(B)]. No amorphous intergranular phase was detected throughout this side of the couple. The intergranular phase consisted of crystallized Y_2SiO_5 and $Zr_3Y_4O_{12}$. These phases were sometimes found as relatively large pockets surrounding β–Si_3N_4 grains (Fig. 11). This is consistent with the observation in the SNA side of the couple of pockets of ZrO_2 grains.

The microstructure of the SNA side, near the surface ($\leqslant 600\ \mu m$), of the SNA/SNY–Si_3N_4 couple was very different to that of the SNA side of the SNA/SNY–ZrO_2 couple (Fig. 12). The microstructure was highly porous and consisted of equiaxed α–Si_3N_4 and β–Si_3N_4 grains. No elongated β–Si_3N_4 grains were observed. The microstructure had the appearance of being only partially sintered, so that the α–Si_3N_4 grains from the starting powder were still apparent.

The microstructure of the SNY side of the SNA/SNY–Si_3N_4 couple was characterized by a high proportion of elongated β–Si_3N_4 grains (Fig. 13). No amorphous intergranular phase was detected. The intergranular phase consisted of crystalline Y-silicate phases.

4. DISCUSSION

The results obtained in the present investigation clearly show the dramatic effect of the ZrO_2 dopant and yttria on the microstructure of alumina–yttria containing silicon nitride compacts. From Figs 1 and 3 it is clear that the Y_2O_3 diffuses $\approx 1000\ \mu m$ into the SNA–ZrO_2 layer, conversely only $50\ \mu m$ in the case of the undoped SNA layer.

It is also observed in Figs 1 and 2 that when ZrO_2 is present in the SNA layer only β–Si_3N_4 was observed. Conversely when this dopant is not present a large fraction of α–Si_3N_4 remains as a metastable phase (Fig. 4). Both facts indicate the drastic effect of the ZrO_2 dopant ($\approx 1.2\%$) on the viscosity of the liquid phase developed at 1750°C in the Si_3N_4–Al_2O_3–SiO_2 system, and consequently its strong effect on the sinterability of the compact as well as the presence of elongated β–Si_3N_4 grains (Figs 5 and 12).

It is also evident from Figs 1 and 2 that in the SNA–ZrO_2 layer, when Y_2O_3 is present even in very low contents ($<0.1\%$) Si_2N_2O is no longer a stable phase.

When both Y_2O_3 and ZrO_2 are present, precipitation of $Zr_3Y_4O_{12}$ occurs (Figs 1 and 2), so that amorphous phases cannot be detected at the grain boundary (Figs 9 and 11). Such a result is significant regarding the high temperature mechanical performance of Si_3N_4-based material [14, 15].

When Al_2O_3, Y_2O_3 and ZrO_2 are present, as in the case of the interface region (Fig. 1) the density increases close to the theoretical value ($>99\%$) but keeps the average grain size of β–Si_3N_4 down to $0.5\ \mu m$ [Fig. 10(A)]. Conversely when alumina is not present as in the case of the SNY inside (Fig. 1), the porosity drastically increases ($\approx 12\%$) but the average grain size [Fig. 10(B)] is then larger ($\approx 1\ \mu m$).

In the SNY layer the presence of ZrO_2 also promotes the precipitation of Y_2SiO_5. In the absence of ZrO_2 the only secondary phase present is the expected

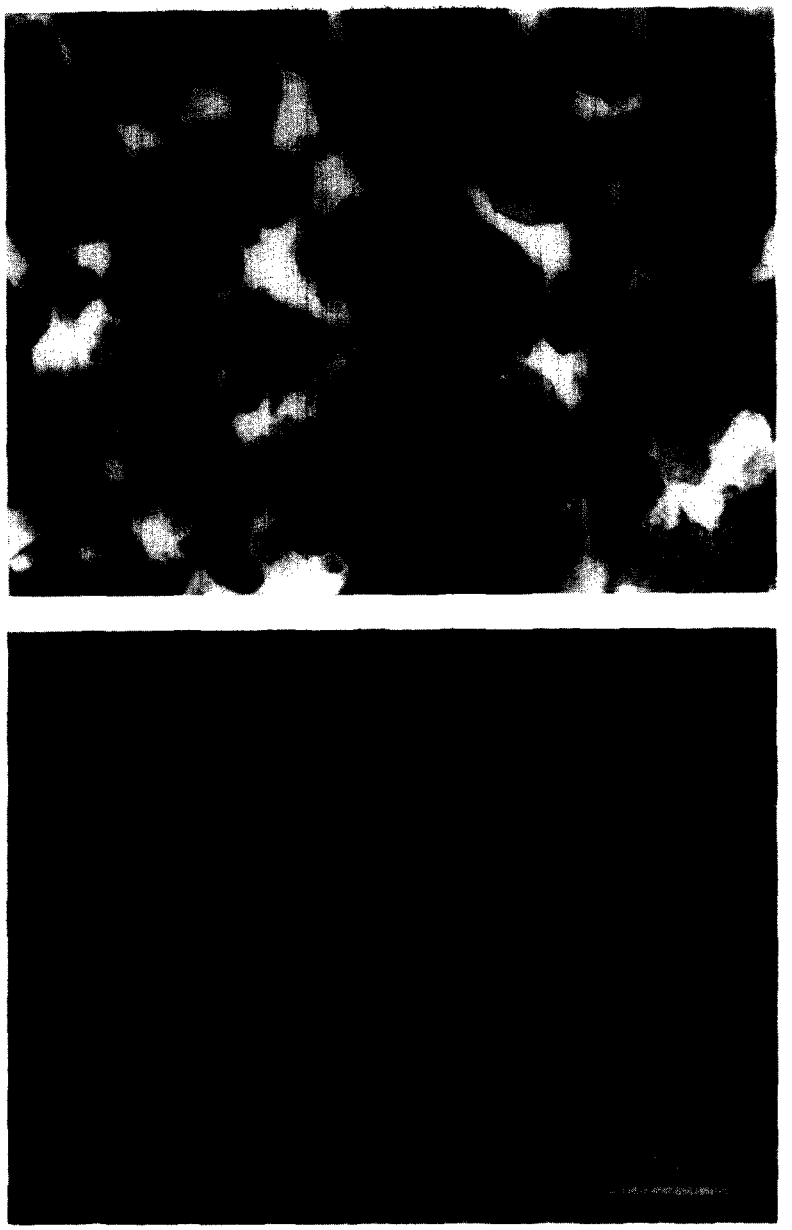

Fig. 12. (A) TEM image of typical microstructure on SNA side, near surface ($\approx 300\,\mu$m), of SNA/SNY–Si_3N_4 couple. (B) SEM of micrograph of the region $\approx 600\,\mu$m from the SNA surface.

$Y_2Si_3N_4O_3$, according to the SiO_2–Y_2O_3–Si_3N_4–YN equilibrium diagram [18], which is detrimental regarding oxidation resistance [14].

5. CONCLUSION

The results obtained in the present investigation have shown that diffusion couples are an appropriate route to study the effect of dopants and additives on the microstructure of Si_3N_4 based materials.

It has been proved that the presence of ZrO_2 drastically decreases the viscosity of the liquid phase developed in Si_3N_4–Al_2O_3 system. Consequently, this fact affects the fraction of β–Si_3N_4 present, the sinterability and average grain size of Si_3N_4 compact. When Y_2O_3 and ZrO_2 are present $Zr_3Y_4O_{12}$ precipitates and the amount of detectable amorphous phase at the grain boundary drastically decreases.

The presence of ZrO_2 in the Si_3N_4–Y_2O_3 system promotes the formation of $Y_2Si_2O_5$ and $Zr_3Y_4O_{12}$ instead of the stable quaternary phase $Y_2Si_3N_4O_3$ which is unwanted regarding oxidation problem. When ZrO_2 and Al_2O_3 are present in this system sinterability increases but the average grain size of β–Si_3N_4 decreases.

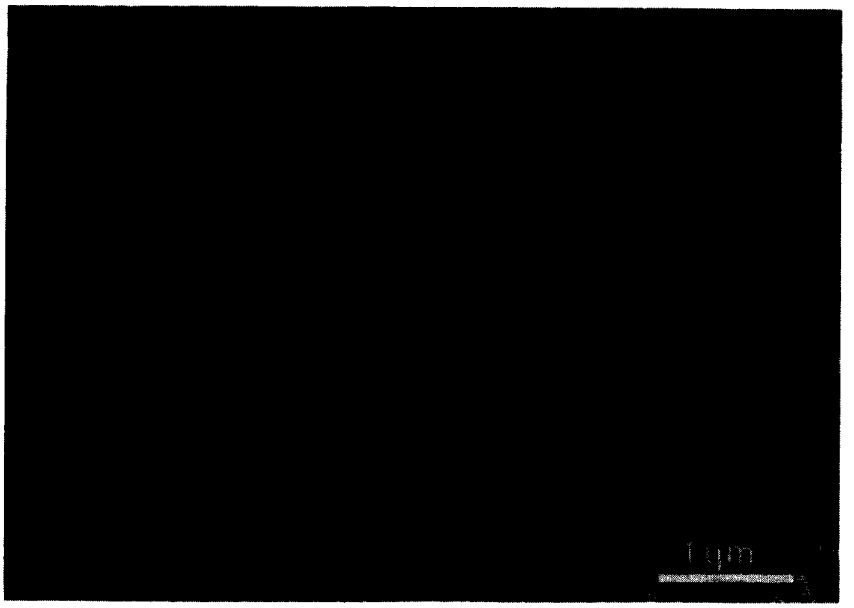

Fig. 13. SEM micrograph showing the plasma etched microstructure of the SNY side of the SNA/SNY–Si_3N_4 couple.

Acknowledgements—This work has been supported by CICYT (Spain) under Project Number MAT-94-0974 and a British/Spanish Joint Research Programme 1994–1995, No. 145B. S. Mello Castanho acknowledges RHAE-CNPq (Brazil) for concession of a grant. We would like to thank Mr L. Lay, National Physical Laboratory, U.K. for his expert assistance with the preparation of the plasma etched specimens. G. Blugan acknowledges The National Physical Laboratory for their support for his studentship. We thank Professor G. Thomas for his helpful discussion.

REFERENCES

1. M. R. Pascucci and R. N. Katz, *Interceram* **42**(2), 71 (1993).
2. C. Sorrel, *J. Austr. Ceram. Soc.* **18**(2), 22 (1983).
3. K. H. Jack, *J. Mater. Sci.* **11**, 1135 (1976).
4. S. Boskovic, *J. Mater. Sci.* **25**, 1513 (1990).
5. A. Tsuge and K. Nishida, *Amer. Cer. Soc. Bull.* **57**(4), 424 (1977).
6. O. Abe, *J. Mater. Sci.* **25**, 3641 (1990).
7. D. Suttor and G. S. Fischmann, *J. Am. Ceram. Soc.* **75**(5), 1063 (1992).
8. F. F. Lange, *Am. Ceram. Soc. Bull.* **62**(12), 1369 (1983).
9. M. K. Cinibulk, G. Thomas and S. M. Johnson, *J. Am. Ceram. Soc.* **75**(8), 2037 (1992).
10. J. C. Almeida, A. T. Fonseca, R. N. Correa and J. L. Baptista, *Mater. Sci. Engng A* **109**, 395 (1989).
11. L. K. L. Falk, *Proc. Int. Conf. on Silicon Nitride-Based Ceramics*, Stuttgart, Germany (edited by M. J. Hoffmann, P. F. Becher and G. Petzow), p. 489 (1993).
12. J. R. Kim and C. H. Kim, *J. Mater. Sci.* **25**, 493 (1990).
13. N. Hirosaki, A. Okada and K. Matoba, *J. Am. Ceram. Soc.* **71**(3), C144–147 (1988).
14. M. K. Cinibulk, G. Thomas and S. M. Johnson, *J. Am. Ceram. Soc.* **75**(8), 2050 (1992).
15. W. A. Sanders and L. E. Gloseclose, *J. Am. Ceram. Soc.* **76**(2), 553 (1993).
16. Y. Goto and G. Thomas, *Ceram. Trans.* **42**, 157 (1994).
17. T. R. Dinger, R. S. Rai and G. Thomas, *J. Am. Ceram. Soc.* **71**(4), 236 (1988).
18. L. J. Gauckler, H. Hohnke and T. Y. Tien, *J. Am. Ceram. Soc.* **63**(1–2), 35 (1980).